Potent Anticarcinoma Activity of the Humanized Anti-CD70 Antibody h1F6 Conjugated to the Tubulin Inhibitor Auristatin via an Uncleavable Linker

Ezogelin Oflazoglu,[1] Ivan J. Stone,[1] Kristine Gordon,[1] Christopher G. Wood,[2] Elizabeth A. Repasky,[3] Iqbal S. Grewal,[1] Che-Leung Law,[1] and Hans-Peter Gerber[1]

Abstract

Purpose: The antitubulin agent monomethyl auristatin F (MMAF) induces potent antitumor effects when conjugated via protease cleavable linkers to antibodies targeting internalizing, tumor-specific cell surface antigens. Humanized 1F6 (h1F6) is a humanized monoclonal antibody targeting CD70, a member of the tumor necrosis factor family that is expressed on hematologic malignancies and carcinomas. Here, we tested h1F6–maleimidocaproyl (mc) MMAF conjugates, consisting of an uncleavable mc linker, for their ability to interfere with the growth of CD70-positive carcinomas.

Experimental Design: To evaluate the optimal drug per antibody ratio, we conjugated either four or eight MMAF molecules to the cysteines that comprise the interchain disulfides of h1F6 and determined antitumor activities *in vitro* and in xenografted mice. The tumor types tested included glioblastoma, patient-derived renal cell carcinoma (RCC) cell isolates, and standard RCC tumor cell lines.

Results: All h1F6-mcMMAF conjugates potently interfered with the growth of all carcinomas *in vitro* and resulted in complete responses of RCC tumors implanted orthotopically or s.c. in mice. *In vitro*, h1F6-mcMMAF(8) was generally more potent than h1F6-mcMMAF(4). However, h1F6-mcMMAF(4) displayed equal or better efficacy than h1F6-mcMMAF(8) when administered to tumor-bearing mice.

Conclusions: We showed that h1F6-mcMMAF conjugates inhibited the growth of human carcinomas and that increased drug loading, while improving potency *in vitro*, did not substantially affect the pharmacodynamic and pharmacokinetic properties *in vivo*. Based on these findings, h1F6-mcMMAF(4), designated SGN-75, has been identified as a potential antibody-drug conjugate for clinical development.

Carcinomas represent ~70% of the estimated new cancer patients in the United States, thus comprising the most frequent tumor type in humans (1). Several monoclonal antibodies interfering with the signaling events regulated by tumor antigens expressed on carcinomas have gained Food and Drug Administration approval in recent years, including trastuzumab (Herceptin) and cetuximab (Erbitux, reviewed in ref. 2). As a consequence, intense genomic and proteomic efforts are being undertaken to identify novel, membrane-associated tumor antigens that are overexpressed on tumors (3, 4). CD70 is a rapidly internalizing cell surface antigen that is expressed by neoplastic cells in non–Hodgkin's lymphoma, multiple myeloma, and Hodgkin's lymphoma (5–7). CD70 is also up-regulated on several carcinomas, including renal cell (7–10), thymic (11), nasopharyngeal (12), as well as glioblastoma and astrocytoma (13). On normal cells, CD70 expression is limited to activated T cells and B cells and is undetectable on normal lymphocytes or parenchymal cells (14); therefore, it is considered an attractive target for cancer immunotherapy.

Therapeutic antibodies mediate antitumor effects by interfering either directly with tumor intrinsic signaling pathways that are regulated by their respective targets and/or indirectly by engaging effector cell functions via their Fc portions following binding to their targets. Several mechanisms involving effector cell–mediated tumor cell killing have been described, including antibody-dependent cellular cytotoxicity and antibody-dependent cellular phagocytosis, in addition to complement-dependent cytotoxicity (reviewed in ref. 15). As exemplified by rituximab (Rituxan), which substantially improves long-term survival rates of non–Hodgkin's lymphoma patients (16), effector cells and complement-dependent cytotoxicity are important for the therapeutic effects of monoclonal antibodies developed for the treatment of hematologic malignancies. In contrast, only a limited number of carcinoma antigens have been described to contribute

Authors' Affiliations: [1]Department of Preclinical Therapeutics, Seattle Genetics, Inc., Bothell, Washington; [2]Department of Urology, The University of Texas M. D. Anderson Cancer Center, Houston, Texas; and [3]Department of Immunology, Roswell Park Cancer Institute, Buffalo, New York

Received 4/9/08; revised 6/5/08; accepted 6/6/08.

Note: Supplementary data for this article are available at Clinical Cancer Research Online (http://clincancerres.aacrjournals.org/).

H-P. Gerber and C-L. Law contributed equally to this work.

Requests for reprints: Hans-Peter Gerber, Seattle Genetics, Inc., 21823 30th Drive Southeast, Bothell, WA 98021. Phone: 425-527-4910; Fax: 425-527-4611; E-mail: hgerber@seagen.com.

© 2008 American Association for Cancer Research.

doi:10.1158/1078-0432.CCR-08-0916

Downloaded from http://aacrjournals.org/clincancerres/article-pdf/14/19/6171/1977004/6171.pdf by guest on 13 August 2024

Translational Relevance

The report describes profound antitumor effects in primary patient tumor cells that were isolated and implanted orthotopically in the subrenal capsule of nude mice. These data were critical for our selection of the lead compound for clinical development, as models using primary patient tumor isolates have the highest predictive values for clinical responses. This report is the first to describe the pharmacodynamic effects of a novel drug linker, consisting of an uncleavable linker and the potent tubulin inhibitor monomethyl auristatin F (MMAF), when tested on human carcinomas. This novel drug linker is markedly different from the previously published linker types, as it is noncleavable, leading to more stable compounds and better pharmacokinetic characteristics. In addition, the effects of increased drug loading on the pharmacokinetic and pharmacodynamic properties of an antibody targeting CD70 were studied. The data reported here were instrumental for the calculation of the therapeutic indexes of various anti-CD70 antibody-drug conjugates, resulting in the selection of a novel therapeutic compound, SGN-75, for development in clinical trials in humans.

functionally to transformation, including the prototypic epidermal growth factor receptor family members HER2/neu and EGFR/HER1. Durable responses following treatment with function blocking antibodies targeting these tumor antigens have been most frequently observed in combination with chemotherapy (17). Such limited single-agent activities of antibodies targeting carcinomas stimulated the pursuit of strategies to enhance their antitumor effects, including antibody-drug conjugates (reviewed in refs. 18, 19). Antibody-drug conjugates consist of a cytotoxic payload conjugated to a targeting antibody and represent a promising new class of compounds for the treatment of solid tumors (20). Several antibody-drug conjugates using the potent antimitotic agents auristatins as the payload are currently being developed preclinically and in early-stage clinical trials (21, 22).

We previously reported that monomethyl auristatin F (MMAF), when attached to the parental murine anti-CD70 antibody 1F6 via the protease cleavable linker valine-citrulline (vc), induces potent, target-specific cellular cytotoxicity against a variety of hematologic tumor cell lines grown in culture (23) and in a model of renal cell carcinoma (RCC) *in vivo* (7). Here, we explore the utility of a humanized 1F6 (h1F6) conjugated to MMAF via an uncleavable maleimidocaproyl (mc) linker with different drug-antibody ratios to inhibit the growth of solid tumors *in vitro* and *in vivo*. We report potent antitumor activities of h1F6-mcMMAF in all models of RCC tested, including primary human RCC tumor isolates grown orthotopically and in a model of glioblastoma, suggesting the broad utility of uncleavable auristatin-based antibody-drug conjugates for the treatment of carcinomas.

Materials and Methods

Cells and reagents. 786-O, Caki-1, and DBTRG05-MG cells were obtained from the American Type Culture Collection and propagated in culture conditions recommended by the manufacturer. UMRC-3 cells were generated as described previously (24). Surgical isolates from RCC patients were obtained under patient consent and institutional review board approval. To generate primary RCC cultures, surgical tumor isolates from patients were minced in MEM supplemented with gentamicin, fungizone, and penicillin-streptomycin. Minced samples were then collected by low-speed centrifugation and transferred to the sample medium containing collagenase (0.1 mg/mL, Sigma), hyaluronidase (0.1 mg/mL, Sigma), and Type IV DNase (0.02 mg/mL, Sigma). Enzymatic dissociation was carried out at 37°C and 5% CO_2 for 4 h. After low-speed centrifugation, dissociated tumor fragments were cultured in MEM supplemented with Earle's salt and glutamine; penicillin-streptomycin; 10% fetal bovine serum; MEM nonessential amino acids; MEM vitamins; insulin, transferrin, and selenium supplement; hydrocortisone (0.4 μg/mL, Sigma); and epidermal growth factors (10 ng/mL). Cell culture medium and growth supplements used in establishing RCC primary cultures were purchased from Invitrogen. Epithelial cells were passaged and phenotyped for surface expression of CD70. A total of four primary RCC cell cultures were established. RCC1 was obtained from a primary RCC tumor. RCC2M and RCC5M were obtained from metastatic RCC tumors. 10896-3p was isolated from a metastatic RCC lesion (pancreatic metastasis). 10896-3p xenografted tumors were processed after resection through the Tissue Procurement Facility of the Roswell Park Cancer Institute. Primary tumors were cut into 2 × 2 mm pieces in tissue culture medium (RPMI 1640) under sterile conditions. Mice were anesthetized by i.p. injection of 0.4 to 0.5 mL Avertin (2.5 g 2,2,2-tribromoethanol) dissolved in 5 mL of 2-methyl-butanol/200 mL H_2O. Individual tumor pieces were implanted s.c. in the abdominal wall mice (1st passage) and monitored for growth. Tumor specimens that grew to a size of 1 cm^3 (8-12 wk) were retrieved and subsequently passaged into recipient mice (2nd passage) and used for experiments.

Cell binding and flow cytometry. h1F6 was generated by humanization of the parental murine antibody 1F6 (7).[4] Apparent cell binding affinities of h1F6 and h1F6-mcMMAF(4) were determined by incubating cells with graded doses of h1F6 or h1F6-mcMMAF(4) followed by secondary detection with a FITC-conjugated $F(ab')_2$ fragment, Fcγ-specific goat anti-human IgG antibody (Jackson Immunoresearch), followed by flow cytometric analysis on a FACScan (BD Biosciences) instrument. For flow cytometry, 2 × 10^5 cells were incubated in monoclonal antibody–containing staining medium (RPMI 1640, 5-10% fetal bovine serum) on ice for 20 to 30 min. Cells were washed, counterstained with FITC-conjugated goat anti-mouse IgG (Jackson ImmunoResearch), followed by an additional wash and fixation in PBS, 1% paraformaldehyde. CD70 copy numbers were determined by quantitative fluorescence-activated cell sorting using the kit provided by DAKO.

Immunohistochemistry. Frozen tissue sections were thawed, air-dried for 2 h, and fixed in acetone for 10 min at -20°C. Endogenous peroxidase activity was blocked using 0.6% H_2O_2 for 15 min, followed by PBS wash. In studies using biotinylated antibodies, slides were treated with successive 30-min avidin block solution (Vector Laboratories) and biotin block solution (Vector Laboratories). Biotinylated murine 2F2 and humanized 1F6 anti-CD70 monoclonal antibodies, control nonbinding IgG (MOPC21), or biotinylated MOPC21 were used at 2 μg/mL and incubated for >18 h at 4°C. After PBS washes, slides were incubated with avidin-biotin complex reagent (Elite kit, Vector Laboratories), and 3,3V-diaminobenzidine reagent (Vector Laboratories) was used for color development. Images were taken using Axiovert 2000 microscope (Zeiss) using either ×10 or ×40 objectives.

Antibody-drug conjugates. Maleimidocaproyl (mc) MMAF was synthesized and conjugated to antibodies as reported previously (23).

[4] McEarchern et al., in press.

Downloaded from http://aacrjournals.org/clincancerres/article-pdf/14/19/6171/1977004/6171.pdf by guest on 13 August 2024

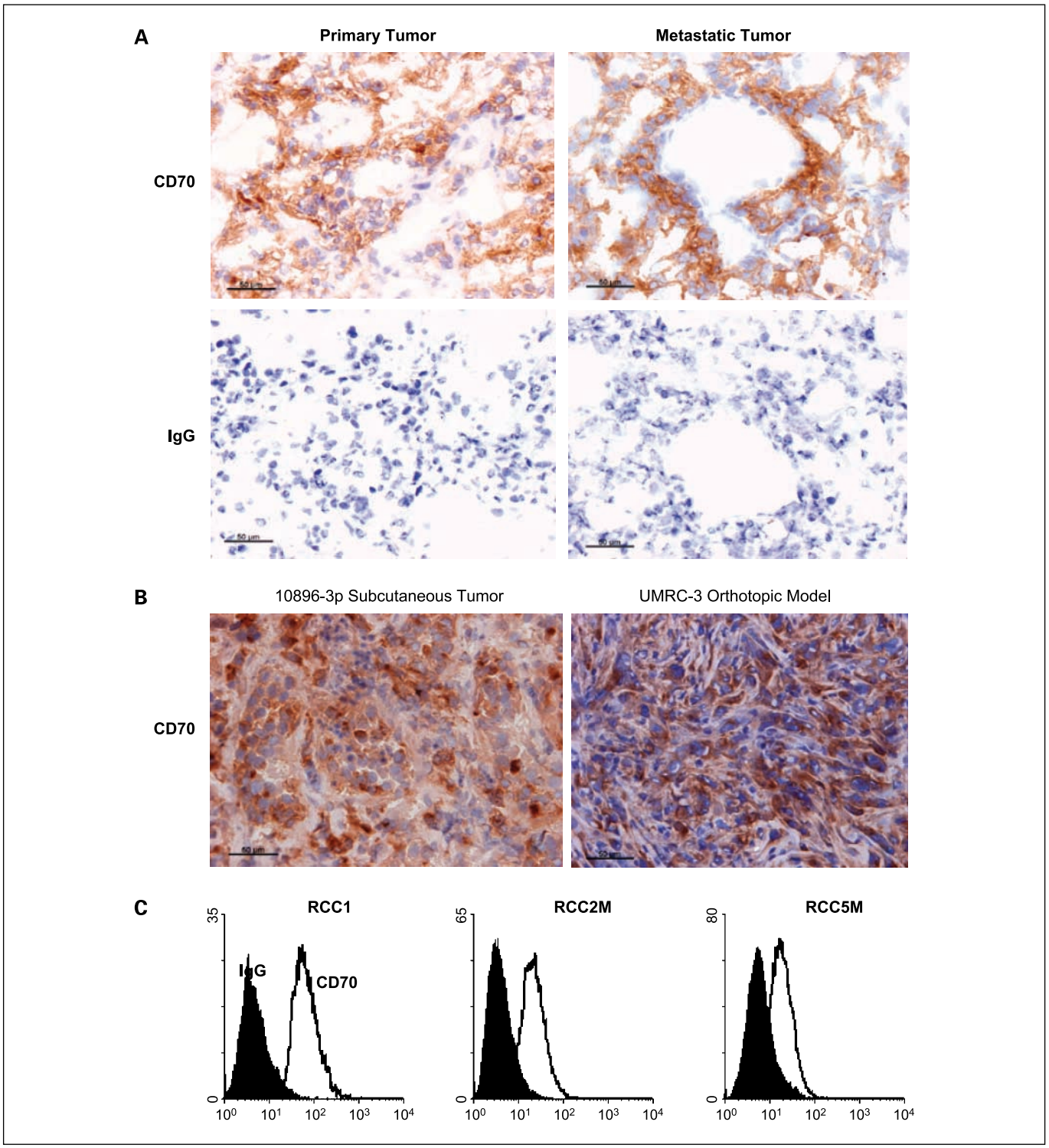

Fig. 1. CD70 is expressed on primary RCC cells. *A,* immunohistochemical staining of frozen tumor sections from primary patient RCC samples was done using an anti-CD70 antibody or a nonbinding IgG-isotype control. Intense CD70 expression (brown 3,3′-diaminobenzidine staining) was observed in primary and metastatic tumor sections (*top*) with no observable background IgG staining (*bottom*). Nuclei were counterstained with hematoxylin (*blue staining*). *B,* immunohistochemical analysis for CD70 expression in 10896-3p RCC tumors grown s.c. (*left*) and UMRC-3 tumors grown orthotopically (*right*) *C,* primary RCC cultures were established from surgical specimens and cell isolates were examined for CD70 expression by flow cytometric analysis using an Alexa Fluor 488–conjugated anti-CD70 antibody and compared with CD70 expression on RCC cell lines.

A mean number of 4 or 8 drug molecules were conjugated per molecule of h1F6 to yield h1F6-mcMMAF(4) or h1F6-mcMMAF(8) conjugates, respectively. Antibody-drug conjugates used in this study typically contained <2% protein aggregates and <0.5% unconjugated free drug.

Cell proliferation and cytotoxicity assays. Cells (500-1,000 per well) were incubated overnight in 100 μL of medium in 96-well flat-bottomed plates. An additional 100 μL of culture medium with varying concentrations of ADCs were added to quadruplicate wells, and

Downloaded from http://aacrjournals.org/clincancerres/article-pdf/14/19/6171/1977004/6171.pdf by guest on 13 August 2024

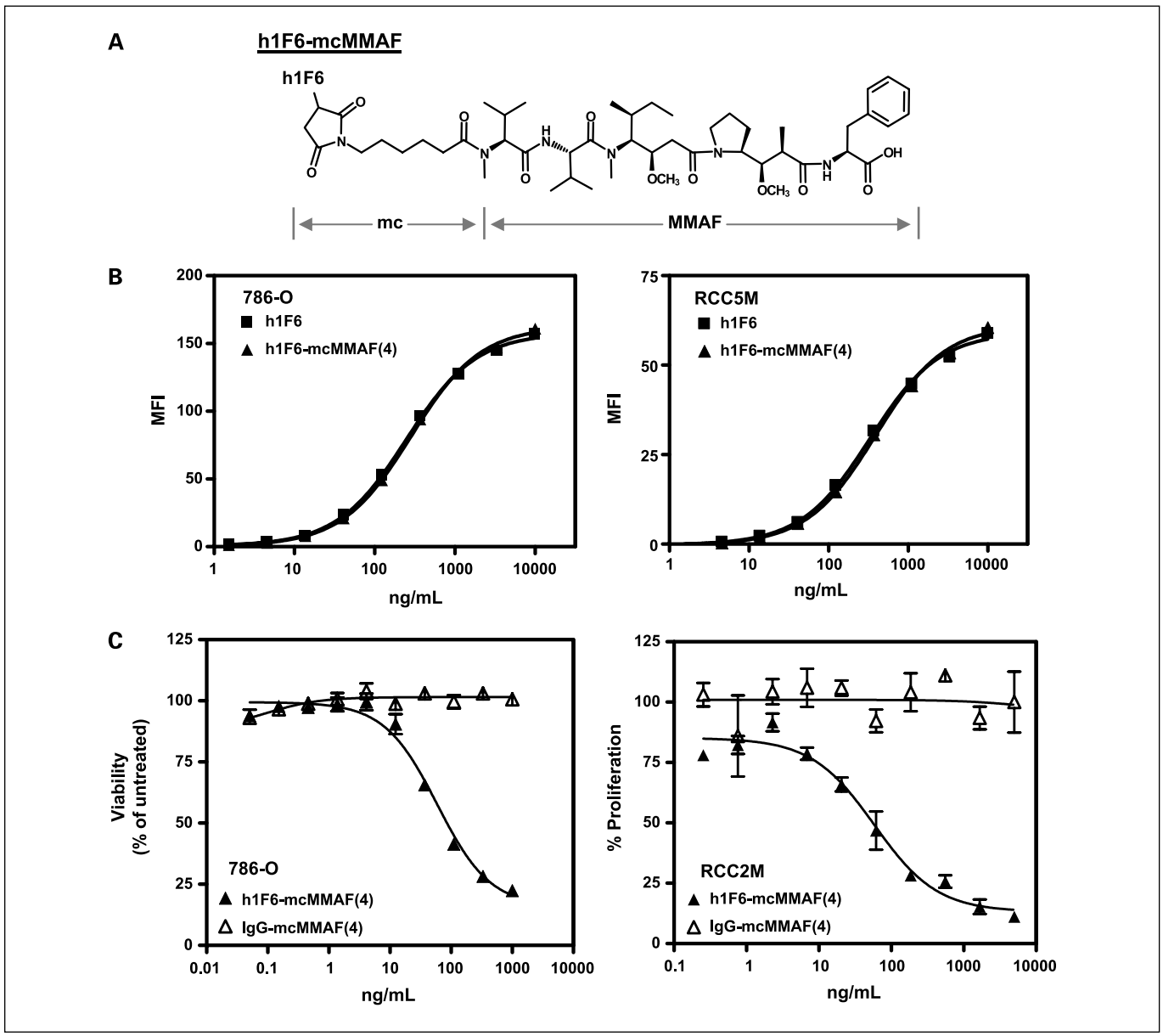

Fig. 2. Structure and binding of h1F6-mcMMAF. *A,* chemical structure of MMAF conjugated via mc linker to a humanized anti-CD70, h1F6. *B,* binding of h1F6 and h1F6-mcMMAF(4) was determined by incubating cells with graded doses of h1F6 or h1F6-mcMMAF conjugates. *C,* viability of 786-O renal carcinoma tumor cells or primary patient tumor isolates from metastatic RCC tumors (RCC2M) incubated for 96 h with graded doses of h1F6-mcMMAF(4) or control antibody-drug conjugate compounds.

incubation was continued for an additional 96 h. Cytotoxicity was assayed by the CellTiter-Glo Cell viability assay (Promega). Proliferation of primary RCC cells (RCC2M) was determined after 96 h by [^{3}H]thymidine incorporation.

Subcutaneous xenograft models. To establish 786-O, UMRC-3, and DBTRG05-MG tumors, 5×10^6 cells were implanted into the right flank of athymic *nu/nu* female donor mice (Harlan). When donor tumors were ~500 mm^3 [$(L \times W^2) / 2$], mice were euthanized, tumors were aseptically excised, and ~0.5 × 0.5 mm fragments were loaded into a sterilized 13-gauge trochar for implantation into anesthetized mice. When tumors reached ~100 or ~300 mm^3 (for treatments of larger tumors), mice were randomly allocated to treatment groups. Tumors were measured twice weekly, and volumes were calculated using the formula $V = (L \times W^2) / 2$. Animals were euthanized when tumors reached ~1,000 mm^3.

Experimental RCC metastasis model. To establish disseminated disease, 2×10^6 UMRC-3 cells were implanted i.p. into CB-17 female severe combined immunodeficient (SCID) mice (Harlan). Treatment with antibody-drug conjugates was initiated 5 d post–tumor implantation. I.p. administration of drug occurred either as 4 injections every 4 days or a total of 10 injections every 4 days, as indicated in the legends. Mice were monitored daily. Body weights and clinical observations were recorded twice weekly and daily following disease onset. Animals were sacrificed when disease symptoms, including bloated abdomen, hunched posture, and scruffiness, manifested, typically starting between days 30 to 40 post–tumor implantation. Weight loss was not prominent and metastatic lesions were observed mainly in the diaphragm and the pancreas.

Orthotopic RCC xenograft models. For implantation in the renal capsule, a 1-in. incision was made on the left lateral side to expose the muscle layer of athymic *nu/nu* female mice. Another 1-in. incision was made to visualize the kidney. Downward pressure was applied on both sides of the incision to exteriorize the kidney. While the medial portion of the kidney was supported with forceps, a separate pair of forceps

Downloaded from http://aacrjournals.org/clincancerres/article-pdf/14/19/6171/1977004/6171.pdf by guest on 13 August 2024

was used to hold the kidney capsule. A small straight forceps end was used to puncture the capsule. The tumor fragment was then placed between the kidney capsule and the exterior of the cortex. The capsule was released and the kidney was returned to normal position. The muscle layer was closed with 4-0 absorbable suture, and the skin was closed with a wound clip. All surgical procedures were done using sterile technique. Seven days postsurgery, wound clips were removed, the mice were randomly allocated to treatment groups, and treatment was initiated 10 days postsurgery.

Assessment of tumor growth and statistical analysis. Tumor quadrupling or triplication times (as indicated) were chosen as time to end point, which were determined by using a nonlinear regression analysis for exponential growth of each individual tumor growth data set from each experimental animal. The tumor quadrupling time was calculated based on the tumor volume at the beginning of treatment. Animals that did not reach the end point were assigned a time to end point value equal to the last day of the study. The percentage of tumor growth delay reflects the delay in reaching time to end point relative to control-treated tumors, which was determined using the formula $\%TGD = [(T - C) / C] \times 100$, where T and C are the median times in days for treated and control groups to reach time to end point using the start of treatment as day 1. Statistical analysis and graphical presentations were conducted using Prism (GraphPad) software for Windows 3.03 software. Median tumor growth curves show group median tumor volumes as a function of time. The log-rank test was used to analyze the significance of the differences between time to end point of treated and control tumor groups, with differences deemed significant (*) at $0.01 \leq P \leq 0.05$ and highly significant (**) at $P \leq 0.01$. For statistical analysis of kidney tumors in the orthotopic model, the Mann-Whitney test of the tumor weights was done. In a complete response, the tumor volume is <13.5 mm^3 for three consecutive measurements during the course of the study. A durable response is defined as the complete absence of palpable tumor during the entire experiment.

Pharmacokinetic analysis of h1F6 antibody-drug conjugates. Single 3-mg/kg dose of h1F6-mcMMAF(4) and 1.5-mg/kg dose of h1F6-mcMMAF (8) were administered i.p. to naive SCID mice ($n = 6$ mice per treatment group). The serum samples were collected at scheduled intervals over a period of 11 weeks to obtain composite pharmacokinetic profiles. The samples were analyzed for antibody-drug conjugate concentrations by a qualified multiplex bead-capture assay using an anti-MMAF antibody. The pharmacokinetic parameters of the antibody-drug conjugate were calculated by noncompartmental and compartmental methods using the WinNonLin v.5.2 (Pharsight) software program. Using the mean estimates of the compartmental parameters from the 3-mg/kg dose group, pharmacokinetic profiles corresponding to a single 1.5-mg/kg dose of h1F6-mcMMAF(4) were simulated, under the assumption of linear pharmacokinetics within the specified dose range.

Results

Expression of CD70 in patient samples and in xenografted RCC tumors in mice. Preclinical tumor models using primary patient tumor isolates have higher values to predict drug response in clinical trials compared with standard tumor cell lines (25). Therefore, we sought to develop orthotopic RCC models using primary patient renal carcinoma cell isolates and to compare the antitumor effects of h1F6 antibody-drug conjugates with conventional tumor cell lines. To validate target gene expression, we conducted immunohistochemical analyses of CD70 expression on sections from primary and metastatic human RCC tumors (Fig. 1A). As reported by us (7) and others previously (8–10), we found intense CD70 expression in primary and metastatic RCC tumor cell lines grown in mice. Strong CD70 expression was also noted on tumors derived from patient cell isolates grown s.c. (Fig. 1B, *left*), which were comparable with the levels observed UMRC-3 tumor (Fig. 1B, *right*). Cell surface expression of CD70 was confirmed by FACS analysis of primary cultures derived from surgical specimens (Fig. 1C). Combined, our findings show that cell surface expression of CD70 is maintained in primary patient tumors grown in mice and validated primary patient–derived tumors and RCC tumor cell lines as suitable preclinical models to determine antitumor activities of anti-CD70 antibody-drug conjugates in xenografted mice.

***Generation of h1F6-mcMMAF(4) and h1F6-mcMMAF(8) conjugates and assessment of their cytotoxic activity* in vitro.** h1F6-mcMMAF(4) and h1F6-mcMMAF(8) conjugates were generated using the mc linker to attach MMAF to h1F6 (Fig. 2A) via a synthesis described previously (23). Binding of h1F6-mcMMAF(4) and h1F6 was determined by incubating tumor cells with increasing concentrations of test compounds, followed by detection with a FITC-conjugated $F(ab')_2$ fragment. h1F6-mcMMAF(4) conjugates bound to CD70$^+$ target cells (786-O and RCC5M) with comparable affinity as unconjugated h1F6 (Fig. 2B). Next, we evaluated the ability of h1F6 antibody-drug conjugates to induce cell death of primary RCC cultures or a panel of CD70$^+$ tumor cell lines (Fig. 2C; Table 1). h1F6-mcMMAF(4), but not nonbinding control IgG-mcMMAF(4), induced dose-dependent cytotoxicity in the RCC cell line 786-O (Fig. 2C, *left*). Likewise, h1F6-mcMMAF(4) inhibited proliferation of the primary RCC culture (RCC2M; IC_{50}, 58 ng/mL; Fig. 2C, *right*), showing that CD70 expressed on RCC tumors

Table 1. IC_{50} values of 1F6 conjugates tested against various human carcinoma cells grown in culture

Cell line	Tumor type	CD70 copy numbers ($\times 10^3$)	IC_{50} (nmol/L)	
			h1F6-mcMMAF(4)	h1F6-mcMMAF(8)
786-O	RCC	190	172 ± 92	19 ± 11
Caki-1	RCC	140	48 ± 42	10 ± 8
Caki-2	RCC	170	369 ± 36	42 ± 20
DBTRG-05MG	GBM	70	20 ± 0.3	ND
U251	GBM	120	15 ± 3	16
L428	HD	105	23 ± 3	46 ± 4
LP-1	MM	34	46 ± 2	155 ± 34

NOTE: Cells were incubated with h1F6-mcMMAF or the corresponding nonbinding controls IgG-mcMMAF at the concentrations indicated. After 96 h of incubation, cell viability was determined using CellTiter-Glo luminescent cell viability reagent. CD70 copy numbers were determined by quantitative FACS analysis.
Abbreviations: ND, not determined; GBM, glioblastoma multiforme; HD, Hodgkin disease; MM, multiple myeloma.

Downloaded from http://aacrjournals.org/clincancerres/article-pdf/14/19/6171/1977004/6171.pdf by guest on 13 August 2024

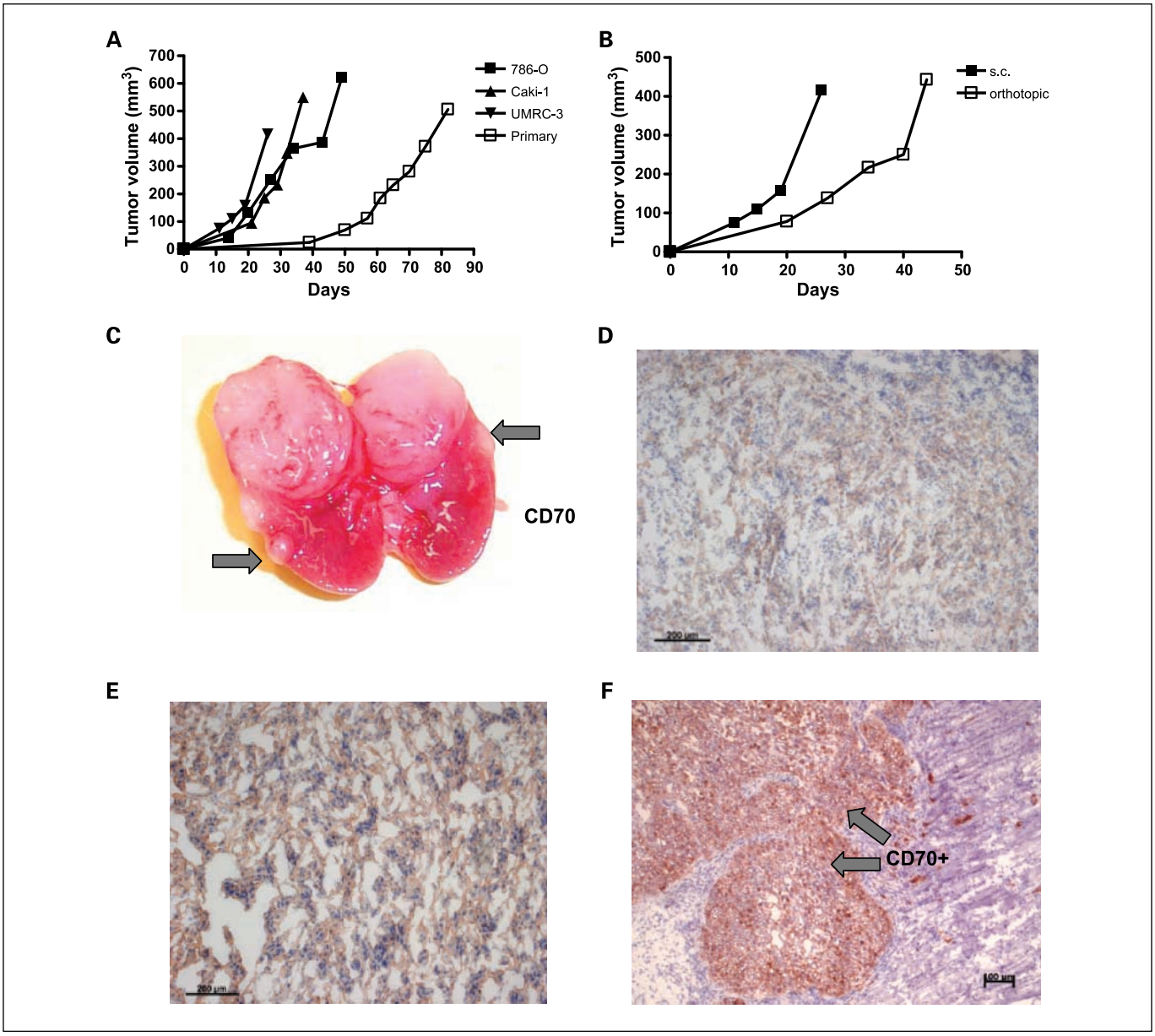

Fig. 3. Growth comparison of RCC xenograft models. *A,* differences in tumor growth rates of RCC cell lines versus primary tumor implants in nude mice ($n = 5$). *B,* differences in UMRC-3 growth when implanted s.c. or orthotopically. *C,* gross pathology of primary tumors in a longitudinal kidney section; arrows, invasive lesions. *D,* immunohistochemical staining of CD70 in sections of 10896-3p tumors grown in the subrenal capsule in SCID mice. Original magnification, ×10. *E,* immunohistochemical staining of CD70 in 786-O tumors grown s.c. in nude mice. Original magnification, ×10. *F,* immunohistochemical analysis of sections from metastatic tumors for CD70 from the diaphragm of SCID mice following i.p. implantation of UMRC-3 tumors.

grown *in situ* has the capacity to internalize h1F6 antibody-drug conjugates. Table 1 summarizes the antitumor effects of h1F6-mcMMAF against a variety of CD70+ tumor cell lines, representing RCC, glioblastoma multiforme, multiple myeloma, and Hodgkin's disease. The IC_{50} values obtained for h1F6-mcMMAF(4) and h1F6-mcMMAF(8) conjugates ranged from 15 to 369 ng/mL and 10 to 155 ng/mL, respectively. In general, h1F6-mcMMAF(8) was found to be more potent than h1F6-mcMMAF(4) on all tumor cell lines tested and no direct correlation between CD70 expression levels and cytotoxic potencies of the conjugates were observed.

RCC model development. h1F6 antibody-drug conjugates were tested in three different models of RCC: s.c. (786-O, UMRC-3), orthotopic (10896-3p, UMRC-3), and in a model of experimental metastasis (UMRC-3). To determine the growth kinetics of primary patient–derived RCC tumor cell isolates (10896-3p), we implanted cells s.c. and compared the antitumor effects with standard tumor cell lines (786-O, Caki-1, UMRC-3; Fig. 3A). Tumors derived from tissue culture cells grew at least 2-fold faster than primary 10896-3p patient cell isolates. When comparing the growth rates of UMRC-3 cells, we found ~2-fold reduced growth in the orthotopic setting, relative to s.c. implantations (Fig. 3B). These findings suggested that the progression of 10896-3p tumors implanted orthotopically into the subrenal capsule of experimental mice was slower compared with standard RCC tumor cell lines, most

Downloaded from http://aacrjournals.org/clincancerres/article-pdf/14/19/6171/1977004/6171.pdf by guest on 13 August 2024

likely caused by the reduced growth rates of primary tumor cell isolates and orthotopically grown tumors. Gross pathologic and immunohistochemical analyses revealed that primary patient samples implanted in the renal capsule were highly invasive (Fig. 3C), reminiscent of the growth of RCC in humans. Expression of CD70 on patient RCC isolates (10896-3p) implanted in the subrenal capsule was confirmed by immunohistochemical analysis of tumor sections (Fig. 3D). Similarly, strong expression of CD70 in sections of 786-O tumors grown s.c. was noted (Fig. 3E). Immunohistochemical analysis of tumors confirmed expression of CD70 on neoplastic cells within metastatic lesions in the pancreas and diaphragm (Fig. 3F) following i.p. injection of UMRC-3 cells. Combined, our studies identified CD70 protein expression in all three experimental models of RCC, validating these models for preclinical studies.

Efficacy of h1F6-mcMMAF conjugates in various models of RCC in mice. First, we investigated the dose-response relationship of h1F6-mcMMAF(4) in three models of RCC and found a dose-dependent inhibition of tumor growth in mice implanted s.c. with 786-O tumors and treated with doses of 1.5 and 4.5 mg/kg (Fig. 4A). Administration of h1F6-mcMMAF(4) at 4.5 mg/kg induced pronounced tumor growth delays, resulting in 2 of 5 durable responses. Substantial reductions in tumor size following treatment with 1.5 mg/kg of h1F6-mcMMAF(4) were found in orthotopically grown primary patient RCC tumor specimens (10896-3p). In these tumors, treatment with 1.5 mg/kg of h1F6-mcMMAF(4) resulted in a

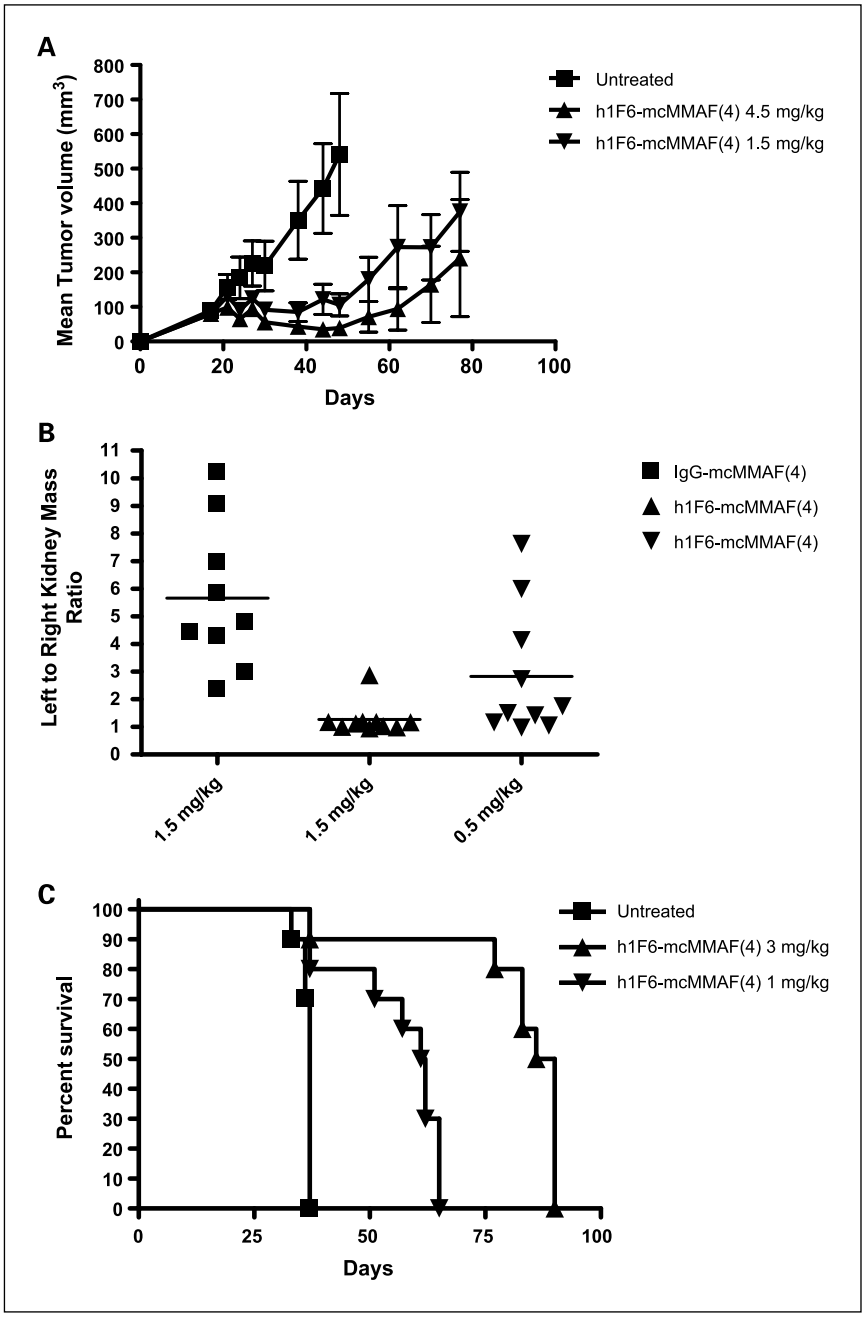

Fig. 4. *In vivo* efficacy of h1F6 antibody-drug conjugates in RCC xenograft models. *A,* 786-O tumors were initiated by implanting tumor fragments (n = 5/group) s.c. in the right flank of athymic *nu/nu* female mice. Treatment was initiated when the average tumor volume reached ~100 mm^3. h1F6-mcMMAF(4) at 4.5 or 1.5 mg/kg was administered i.p. at 7 injections every 4 d, beginning on day 17 after tumor implantation (*arrow*). Points, mean tumor volumes; bars, SE. *B,* primary tumor fragments 10896-3p were implanted orthotopically in the kidney of athymic *nu/nu* female (n = 9-10 per group). h1F6-mcMMAF(4) at 1.5 or 0.75 mg/kg and nonbinding control antibody-drug conjugate at 1.5 mg/kg were administered i.p. at 10 injections every 4 d, beginning on day 10 after tumor implantation. Kidneys were removed on day 68, and left to right kidney mass ratio was measured. *C,* 2×10^6 UMRC-3 tumor cells were implanted i.p. in SCID mice to establish the experimental metastasis model (n = 10 per group). h1F6-mcMMAF(4) at 3 or 1 mg/kg was administered i.p. at 4 injections every 4 d, beginning on day 5 after tumor implantation. Data are Kaplan-Meier survival curves.

Downloaded from http://aacrjournals.org/clincancerres/article-pdf/14/19/6171/1977004/6171.pdf by guest on 13 August 2024

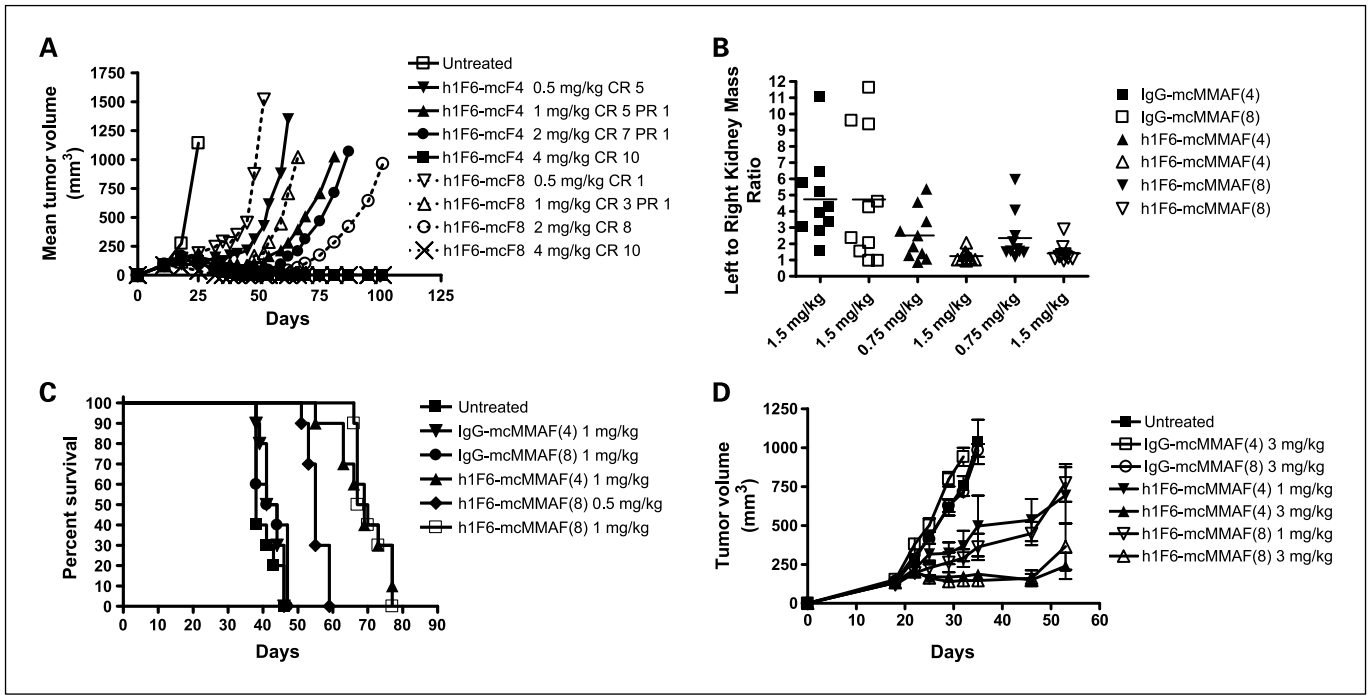

Fig. 5. Antitumor effects of h1F6 conjugates with different drug loadings against carcinomas. *A,* tumor growth curves of 786-O tumors implanted in athymic *nu/nu* female mice (n = 10 per group). Treatment was initiated when tumors reached 100 mm^3 (4 injections every 4 d; i.p.). *B,* primary tumor fragments were implanted in kidneys of athymic *nu/nu* female mice (n = 10/group). h1F6 antibody-drug conjugates and nonbinding control antibody-drug conjugates were administered i.p. at 10 injections every 4 d, beginning on day 10 after tumor implantation. Kidneys were removed on day 68, and left to right kidney mass ratios were determined. *C,* UMRC-3 cells were implanted i.p. in SCID mice and h1F6 conjugates were administered i.p., 4 injections every 4 d, starting on day 5 after tumor implantation. Data represent the Kaplan-Meier survival curves. *D,* DBTRG-05MG glioblastoma tumor fragments were implanted in athymic *nu/nu* female mice (n = 6 per group). Treatment was initiated when average tumor volumes reached ~100 mm^3. h1F6 antibody-drug conjugates and nonbinding control antibody-drug conjugates were administered at 3 or 1 mg/kg, i.p., 4 injections every 4 d, beginning on day 18 after tumor implantation (*arrow*).

significant decrease in left-to-right kidney mass ratios and substantially reduced tumor growth rates compared with treatment with a nonbinding control–antibody-drug conjugate compound ($P < 0.05$; Fig. 4B). Distant metastases are common in RCC and nearly one fourth of the patients display metastases at presentation whereas another 50% develop metastases during the follow-up (26, 27). To assess the therapeutic effects of h1F6 antibody-drug conjugates on tumor dissemination, we developed a model of experimental RCC metastasis. Implantation of UMRC-3 cells i.p. resulted in metastatic lesions in the pancreas and diaphragm, starting from day 30 postimplantation. Tumor dissemination and growth was associated with a rapid decrease in survival, reaching 100% penetrance by day 40 (Fig. 4C and data not shown, respectively). We found that treatment of i.p. implanted UMRC-3 tumors with h1F6-mcMMAF(4) resulted in a significant and dose-dependent increase in survival relative to untreated mice ($P < 0.005$; Fig. 4C). In summary, these data show that the h1F6-mcMMAF(4) conjugates induced potent, dose-dependent anticarcinoma activities in all experimental models tested. We established the target dose range for subsequent lead identification studies to be between 0.5 and 4.5 mg/kg.

Efficacy of h1F6 antibody-drug conjugates with different drug loading ratios in models of RCC and glioblastoma multiforme. Variations in drug loading may affect potency and/or efficacy of anti-CD70 antibody-drug conjugates. In support of this notion, experiments *in vitro* suggested that h1F6-mcMMAF(8) conjugates were more potent than h1F6-mcMMAF(4) at inducing tumor cell death (Table 1). To evaluate the effect of drug load *in vivo*, we tested the antitumor effects of h1F6 mcMMAF(4) and h1F6 mcMMAF(8) conjugates in all three RCC models developed. Based on antibody dose levels, both compounds induced similar degrees of tumor growth delay when tested against s.c. implanted 786-O tumors, despite the nominal 2-fold increase in drug equivalents per antibody of the mcMMAF(8) conjugate (Fig. 5A). Similarly, 4- and 8-loaded compounds induced comparable degrees of tumor inhibition at the 0.75- and 1.5-mg/kg dose levels (P = 1.0 and 0.315, respectively; Fig. 5B) when tested against primary patient samples implanted orthotopically. Studies using the UMRC-3 experimental RCC metastasis model show that both the h1F6-mcMMAF(8) and h1F6-mcMMAF(4) conjugates induced significant increases in the survival of mice implanted with tumors ($P < 0.0001$ for both antibody-drug conjugates), with both conjugates displaying comparable efficacies [P = 0.9558; 1 mg/kg; h1F6-mcMMAF(4) versus (8); Fig. 5C].

We further evaluated whether the pharmacodynamic effects of h1F6 antibody-drug conjugates were unique for RCC tumors or whether other tumor types would also be affected. For this purpose, we implanted a CD70-positive glioblastoma cell line DBTRG-05MG s.c. into nude mice followed by the administration of h1F6-mcMMAF conjugates. Similar to our findings in RCC models, h1F6-mcMMAF(4) and h1F6-mcMMAF(8) conjugates were equally effective at interfering with the growth of glioblastoma tumors (Fig. 5D), when assessed based on antibody dose levels. Combined, our studies show that h1F6-mcMMAF(4) and h1F6-mcMMAF(8)

Downloaded from http://aacrjournals.org/clincancerres/article-pdf/14/19/6171/1977004/6171.pdf by guest on 13 August 2024

conjugates inhibited the growth of different carcinomas to similar extents. Statistical analysis of the tumor growth inhibition rates indicated that mcMMAF(4) compounds are at least equal to or more potent than mcMMAF(8) compounds, based on antibody dose levels (Fig. 5A-D). To calculate the levels of drug exposure in SCID mice, the pharmacokinetic properties of h1F6-mcMMAF(8) and mcMMAF(4) conjugates were determined. As shown in Supplementary Table S1, both compounds displayed comparable pharmacokinetic characteristics, with serum half-lives of 12.8 and 14.1 days for 4- and 8-loaded compounds, respectively. These findings suggest that increased drug loading of h1F6 conjugates consisting of noncleavable linkers is not associated with faster clearance rates. Therefore, the equipotency at similar antibody dose levels of h1F6 conjugates are unlikely to be caused by differences in their exposure levels in mice.

Discussion

Despite substantial improvements in the treatment of early-stage carcinomas, most patients with advanced-stage disease will eventually relapse and progress rapidly. The lack of effective salvage treatment options represents a substantially unmet medical need in the treatment of refractory carcinomas. Antibody-drug conjugates combine antibody selectivity with drug cell-killing potency and therefore may represent useful options for the treatment of early- and late-stage carcinomas (28). When tested preclinically, several types of antibody-drug conjugates have been shown to induce potent antitumor effects, including maytansinoids, auristatins, calicheamicin, and doxorubicin derivatives (29). Most of these experiments were conducted with antibody-drug conjugates consisting of either cleavable linkers (7, 30, 31) or acid-sensitive, hydrazone-based linkers (22, 32, 33). In this report, we show that an antibody-drug conjugate consisting of the humanized anti-CD70 antibody h1F6 linked to the antimitotic agent MMAF via an uncleavable mc linker – induced potent antitumor responses, including the complete regressions of experimental RCCs. Our data show that auristatin-based antibody-drug conjugates using an uncleavable linker have utility for the treatment of human carcinomas.

Biochemical analysis of internalized mcMMAF antibody-drug conjugates identified an intracellular catabolic process associated with the degradation of internalized antibody-drug conjugates, leading to the generation of the active cysteine adduct cys-mcMMAF within tumor cells (23). Importantly, the active adducts released from vcMMAF and mcMMAF conjugates differ greatly in their uptake and retention by their cellular targets, with mcMMAF conjugates accumulating more prominently in tumor versus normal tissues when compared with vcMMAF (34). In support of these findings, preliminary tolerability studies in mice evaluating "off-target" toxicity revealed comparable maximal tolerated doses between h1F6-mcMMAF(8) and h1F6-mcMMAF(4) antibody-drug conjugates in the range of >150 mg/kg in single-dose experiments (data not shown). These levels are favorable compared with the ~50 mg/kg maximal tolerated dose of vcMMAF conjugates reported previously (23). However, the safety and efficacy characteristics of antibody-drug conjugates may vary between tumor types; therefore, it is important to evaluate optimal drug-linker combinations for each tumor type and antigen individually.

When tested for antitumor activity *in vitro*, we found h1F6-mcMMAF(8) conjugates to be substantially more potent than h1F6-mcMMAF(4) derivatives (Table 1). More generally, the therapeutic benefit provided by auristatin-based antibody-drug conjugates has been shown to directly correlate with drug loading, independent of the antibody context, when tested against various tumor cell lines of hematopoietic origin *in vitro* (35, 36). However, the *in vivo* antitumor activities of h1F6-mcMMAF(4) and h1F6-mcMMAF(8) conjugates in models of RCC and glioblastoma were comparable (Fig. 5A-D). Similar conclusions were drawn from studies investigating the anti-CD30 antibody cAC10 conjugated with increasing equivalents of the structurally related monomethylauristatin E (37). Finally, a lack of correlation between the *in vitro* and *in vivo* activities of maytansinoid-based antibody-drug conjugates has been reported, indicating that these observations are independent of the antibody, model, and the chemotype tested (32, 33). The cause for such inconsistencies between *in vitro* and *in vivo* antitumor activities of antibody-drug conjugates has not been clearly established. However, the difference in the pharmacokinetic properties may eventually explain these findings. Whereas further pharmacokinetic studies are required to determine the exposure levels of h1F6 antibody-drug conjugates more conclusively, preliminary pharmacokinetic analysis in mice revealed similar plasma clearance rates of h1F6-mcMMAF(4) and h1F6-mcMMAF(8) antibody-drug conjugates, arguing against the possibility that the higher loaded species are cleared faster (Supplementary Table S1). Finally, it is likely that biological parameters known to be involved in antibody-drug conjugate activity, including target expression levels and internalization rates, cellular trafficking to lysosomal compartments, the composition of the extracellular matrix, and the tubulin architecture, are regulated differently in tumor cells grown *in vitro* versus *in vivo*. In conclusion, *in vitro* studies provide only limited value and data from *in vivo* studies are more relevant for the identification of the optimal drug-linker combinations for different therapeutic targets.

To generate preclinical efficacy data that is predictive of clinical outcome, development of tumor models that most closely mimic human conditions is paramount (ref. 25; reviewed in ref. 38). Tumor models using primary patient RCC cell isolates, in particular when implanted orthotopically in the subrenal capsule, were shown to predict efficacy of compounds in the clinic with high accuracy (25, 39–41). In this report, we describe the development of orthotopic RCC models using primary patient RCC tumor cell isolates. Our data show moderate to high levels of CD70 expression in tumors derived from primary patient RCC cell isolates, which were comparable with the levels observed in tumors derived from standard tumor cell lines. When tested in these models, anti-CD70 auristatin conjugates consisting of an uncleavable linker induced potent antitumor effects, resulting in complete tumor regressions starting at dose levels of 0.5 mg/kg. Importantly, the conjugates described in this report consist of a noncleavable (mc) linker. These compounds carry the potential of reduced off-target toxicity, based on the more selective drug release following internalization into the target cancer cell. In support of this notion, the mc-MMAF

Downloaded from http://aacrjournals.org/clincancerres/article-pdf/14/19/6171/1977004/6171.pdf by guest on 13 August 2024

conjugates seem to be better tolerated in the context of the anti-CD70 antibody compared with the previously published, protease cleavable vc linker–based conjugates (23). Importantly, comparable exposure levels were measured for 8- and 4-loaded mcMMAF compounds. Given the reduced tolerability of higher loaded antibody-drug conjugates described previously (37) and the equipotency between 4- and 8-loaded compounds identified in this report, the h1F6-mcMMAF(4) conjugate, designated as SGN-75, provides superior therapeutic indexes and warrants clinical development in solid tumor indications.

Disclosure of Potential Conflicts of Interest

C. Law has applied for patent anti-CD70 conjugates in the treatment of CD70 expressing cancers. E. Oflazoglu, I. Stone, I. Grewal, C. Law, K. Gordon, and H. Gerber are employed by Seattle Genetics, Inc.

Acknowledgments

We thank Kim Kissler, Jamie Miyamoto, Damon Meyer, Carmel Lynch, and Leia Smith for their contributions to this manuscript; Bhaskar Rege, Gerald Neslund, and Dawn Hayes for their help in pharmacokinetic analysis; and Steve Alley, Julie McEarchern, Paul Carter, and Peter Senter for the critical reading of the manuscript.

References

1. Jemal A, Siegel R, Ward E, Murray T, Xu J, Thun MJ. Cancer statistics, 2007. CA Cancer J Clin 2007;57:43–66.
2. Reichert JM, Valge-Archer VE. Development trends for monoclonal antibody cancer therapeutics. Nat Rev Drug Discov 2007;6:349–56.
3. Carter P, Smith L, Ryan M. Identification and validation of cell surface antigens for antibody targeting in oncology. Endocr Relat Cancer 2004;11:659–87.
4. Papkoff J. New solid tumor targets for therapeutic monoclonal antibodies. Expert Opin Ther Targets 2007;11:585–8.
5. Gruss HJ, Kadin ME. Pathophysiology of Hodgkin's disease: functional and molecular aspects. Baillieres Clin Haematol 1996;9:417–46.
6. Hsu SM, Waldron J, Xie SS, Hsu PL. Hodgkin's disease and anaplastic large cell lymphoma revisited. 1. Unique cytokine and cytokine receptor profile distinguished from that of non-Hodgkin's lymphomas. J Biomed Sci 1995;2:302–13.
7. Law CL, Gordon KA, Toki BE, et al. Lymphocyte activation antigen CD70 expressed by renal cell carcinoma is a potential therapeutic target for anti-CD70 antibody-drug conjugates. Cancer Res 2006;66:2328–37.
8. Diegmann J, Junker K, Gerstmayer B, et al. Identification of CD70 as a diagnostic biomarker for clear cell renal cell carcinoma by gene expression profiling, real-time RT-PCR and immunohistochemistry. Eur J Cancer 2005;41:1794–801.
9. Adam PJ, Terrett JA, Steers G, et al. CD70 (TNFSF7) is expressed at high prevalence in renal cell carcinomas and is rapidly internalised on antibody binding. Br J Cancer 2006;95:298–306.
10. Junker K, Hindermann W, von Eggeling F, Diegmann J, Haessler K, Schubert J. CD70: a new tumor specific biomarker for renal cell carcinoma. J Urol 2005;173:2150–3.
11. Hishima T, Fukayama M, Hayashi Y, et al. CD70 expression in thymic carcinoma. Am J Surg Pathol 2000;24:742–6.
12. Agathanggelou A, Niedobitek G, Chen R, Nicholls J, Yin W, Young LS. Expression of immune regulatory molecules in Epstein-Barr virus-associated nasopharyngeal carcinomas with prominent lymphoid stroma. Evidence for a functional interaction between epithelial tumor cells and infiltrating lymphoid cells. Am J Pathol 1995;147:1152–60.
13. Held-Feindt J, Mentlein R. CD70/CD27 ligand, a member of the TNF family, is expressed in human brain tumors. Int J Cancer 2002;98:352–6.
14. Hintzen RQ, Lens SM, Koopman G, Pals ST, Spits H, van Lier RA. CD70 represents the human ligand for CD27. Int Immunol 1994;6:477–80.
15. Carter PJ. Potent antibody therapeutics by design. Nat Rev Immunol 2006;6:343–57.
16. Clynes RA, Towers TL, Presta LG, Ravetch JV. Inhibitory Fc receptors modulate *in vivo* cytotoxicity against tumor targets. Nat Med 2000;6:443–6.
17. Lollini PL, Nicoletti G, Landuzzi L, De Giovanni C, Nanni P. New target antigens for cancer immunoprevention. Curr Cancer Drug Targets 2005;5:221–8.
18. Presta LG. Selection, design, and engineering of therapeutic antibodies. J Allergy Clin Immunol 2005;116:731–6; quiz 7.
19. Wu AM, Senter PD. Arming antibodies: prospects and challenges for immunoconjugates. Nat Biotechnol 2005;23:1137–46.
20. Polakis P. Arming antibodies for cancer therapy. Curr Opin Pharmacol 2005;5:382–7.
21. Francisco JA, Cerveny CG, Meyer DL, et al. cAC10-vcMMAE, an anti-CD30-monomethyl auristatin E conjugate with potent and selective antitumor activity. Blood 2003;102:1458–65.
22. Doronina SO, Toki BE, Torgov MY, et al. Development of potent monoclonal antibody auristatin conjugates for cancer therapy. Nat Biotechnol 2003;21:778–84.
23. Doronina SO, Mendelsohn BA, Bovee TD, et al. Enhanced activity of monomethylauristatin F through monoclonal antibody delivery: effects of linker technology on efficacy and toxicity. Bioconjug Chem 2006;17:114–24.
24. Copland JA, Luxon BA, Ajani L, et al. Genomic profiling identifies alterations in TGFβ signaling through loss of TGFβ receptor expression in human renal cell carcinogenesis and progression. Oncogene 2003;22:8053–62.
25. Fiebig HH, Maier A, Burger AM. Clonogenic assay with established human tumour xenografts: correlation of *in vitro* to *in vivo* activity as a basis for anticancer drug discovery. Eur J Cancer 2004;40:802–20.
26. Healy KA, Marshall FF, Ogan K. Cytoreductive nephrectomy in metastatic renal cell carcinoma. Expert Rev Anticancer Ther 2006;6:1295–304.
27. Pantuck AJ, Belldegrun AS, Figlin RA. Cytoreductive nephrectomy for metastatic renal cell carcinoma: is it still imperative in the era of targeted therapy? Clin Cancer Res 2007;13:693–6s.
28. Ricart AD, Tolcher AW. Technology insight: cytotoxic drug immunoconjugates for cancer therapy. Nat Clin Pract Oncol 2007;4:245–55.
29. Pastan I, Hassan R, Fitzgerald DJ, Kreitman RJ. Immunotoxin therapy of cancer. Nat Rev Cancer 2006;6:559–65.
30. Tse KF, Jeffers M, Pollack VA, et al. CR011, a fully human monoclonal antibody-auristatin E conjugate, for the treatment of melanoma. Clin Cancer Res 2006;12:1373–82.
31. Ross S, Spencer SD, Holcomb I, et al. Prostate stem cell antigen as therapy target: tissue expression and *in vivo* efficacy of an immunoconjugate. Cancer Res 2002;62:2546–53.
32. Erickson HK, Park PU, Widdison WC, et al. Antibody-maytansinoid conjugates are activated in targeted cancer cells by lysosomal degradation and linker-dependent intracellular processing. Cancer Res 2006;66:4426–33.
33. Kovtun YV, Audette CA, Ye Y, et al. Antibody-drug conjugates designed to eradicate tumors with homogeneous and heterogeneous expression of the target antigen. Cancer Res 2006;66:3214–21.
34. Alley SC, Zhang X, Okeley NM, et al. Effects of linker chemistry on tumor targeting by anti-CD70 antibody-drug conjugates [abstract 916]. Proc AACR 2007;48:3812.
35. Sun MM, Beam KS, Cerveny CG, et al. Reduction-alkylation strategies for the modification of specific monoclonal antibody disulfides. Bioconjug Chem 2005;16:1282–90.
36. McDonagh CF, Turcott E, Westendorf L, et al. Engineered antibody-drug conjugates with defined sites and stoichiometries of drug attachment. Protein Eng Des Sel 2006;19:299–307.
37. Hamblett KJ, Senter PD, Chace DF, et al. Effects of drug loading on the antitumor activity of a monoclonal antibody drug conjugate. Clin Cancer Res 2004;10:7063–70.
38. Suggitt M, Bibby MC. 50 years of preclinical anticancer drug screening: empirical to target-driven approaches. Clin Cancer Res 2005;11:971–81.
39. Langdon SP, Hendriks HR, Braakhuis BJ, et al. Preclinical phase II studies in human tumor xenografts: a European multicenter follow-up study. Ann Oncol 1994;5:415–22.
40. Teicher BA. Tumor models for efficacy determination. Mol Cancer Ther 2006;5:2435–43.
41. Sausville EA, Burger AM. Contributions of human tumor xenografts to anticancer drug development. Cancer Res 2006;66:3351–4.

Downloaded from http://aacrjournals.org/clincancerres/article-pdf/14/19/6171/1977004/6171.pdf by guest on 13 August 2024